4-5-2023

Spatiotemporally dynamic electric fields for brain cancer treatment: an in vitro investigation

Erin Iredale

Abdulla Elsaleh

Hu Xu

Paul Christiaans

Andrew Deweyert

See next page for additional authors

IOP Publishing Phys. Med. Biol. 68 (2023) 085012 https://doi.org/10.1088/1361-6560/acc308

Physics in Medicine & Biology

IPEM Institute of Physics and Engineering in Medicine

OPEN ACCESS

RECEIVED
7 December 2022

REVISED
17 February 2023

ACCEPTED FOR PUBLICATION
9 March 2023

PUBLISHED
5 April 2023

PAPER

Spatiotemporally dynamic electric fields for brain cancer treatment: an *in vitro* investigation

Erin Iredale[1,*], Abdulla Elsaleh[2], Hu Xu[3], Paul Christiaans[4], Andrew Deweyert[5], John Ronald[1,6], Susanne Schmid[7], Matthew O Hebb[3,7], Terry M Peters[1,6] and Eugene Wong[1,4]

[1] Department of Medical Biophysics, Schulich School of Medicine and Dentistry, Western University, London, ON, Canada
[2] Department of Physiology and Pharmacology, Schulich School of Medicine and Dentistry, Western University, London, ON, Canada
[3] Department of Clinical Neurological Sciences, Schulich School of Medicine and Dentistry, Western University, London, ON, Canada
[4] Department of Physics and Astronomy, Western University, London, ON, Canada
[5] Department of Medical Education, Northwestern Feinberg School of Medicine, Chicago, IL, United States of America
[6] Robarts Research Institute, Western University, London, ON, Canada
[7] Department of Anatomy and Cell Biology, Schulich School of Medicine and Dentistry, Western University, London, ON, Canada
[*] Author to whom any correspondence should be addressed.

E-mail: eiredale@uwo.ca

Keywords: electrotherapy, electric field, glioblastoma, glioma, brain cancer

Supplementary material for this article is available online

Abstract

Objective. The treatment of glioblastoma (GBM) using low intensity electric fields (~1 V cm^{-1}) is being investigated using multiple implanted bioelectrodes, which was termed intratumoral modulation therapy (IMT). Previous IMT studies theoretically optimized treatment parameters to maximize coverage with rotating fields, which required experimental investigation. In this study, we employed computer simulations to generate spatiotemporally dynamic electric fields, designed and purpose-built an IMT device for *in vitro* experiments, and evaluated the human GBM cellular responses to these fields. *Approach*. After measuring the electrical conductivity of the *in vitro* culturing medium, we designed experiments to evaluate the efficacy of various spatiotemporally dynamic fields: (a) different rotating field magnitudes, (b) rotating versus non-rotating fields, (c) 200 kHz versus 10 kHz stimulation, and (d) constructive versus destructive interference. A custom printed circuit board (PCB) was fabricated to enable four-electrode IMT in a 24-well plate. Patient derived GBM cells were treated and analyzed for viability using bioluminescence imaging. *Main results*. The optimal PCB design had electrodes placed 6.3 mm from the center. Spatiotemporally dynamic IMT fields at magnitudes of 1, 1.5, and 2 V cm^{-1} reduced GBM cell viability to 58%, 37% and 2% of sham controls respectively. Rotating versus non-rotating, and 200 kHz versus 10 kHz fields showed no statistical difference. The rotating configuration yielded a significant reduction ($p < 0.01$) in cell viability (47 $\pm$ 4%) compared to the voltage matched (99 $\pm$ 2%) and power matched (66 $\pm$ 3%) destructive interference cases. *Significance*. We found the most important factors in GBM cell susceptibility to IMT are electric field strength and homogeneity. Spatiotemporally dynamic electric fields have been evaluated in this study, where improvements to electric field coverage with lower power consumption and minimal field cancellations has been demonstrated. The impact of this optimized paradigm on cell susceptibility justifies its future use in preclinical and clinical trial investigations.

Introduction

New treatments for glioblastoma (GBM) are imperative, as it remains the most common incurable primary brain cancer (Nam and de Groot 2017). The clinical treatment standard for GBM is currently surgical resection followed by concurrent chemotherapy (temozolomide) and radiotherapy (Nam and de Groot 2017), but survival outcomes remain poor. Advancements in the field of electrotherapy have given rise to the use of low

intensity, non-ablative electric fields to control the growth of brain tumors (Kirson *et al* 2007, Hottinger *et al* 2016, Swanson *et al* 2016, Xu *et al* 2016, Lok *et al* 2017, Di Sebastiano *et al* 2018, Deweyert *et al* 2019, Fabian *et al* 2019, Shah *et al* 2020). Our group has shown that the delivery of tumor suppressing electric fields using implantable bioelectrodes, termed intratumoral modulation therapy (IMT), is efficacious in preclinical investigations (Xu *et al* 2016, Di Sebastiano *et al* 2018, Deweyert *et al* 2019) using a single stimulating electrode. Electric fields of intermediate frequency (200 kHz) produced from low voltage (2 V) sources impede the growth of high grade gliomas, including GBM, while non-neoplastic neurons and brain tissue remains relatively unaffected (Di Sebastiano *et al* 2018, Deweyert *et al* 2019). We and others have demonstrated computer simulations to be useful tools to analyze and plan electric field distributions in realistic preclinical and clinical scenarios (Miranda *et al* 2014, Wenger *et al* 2015, 2015, Korshoej *et al* 2016, 2017, Wenger *et al* 2018, Iredale *et al* 2020, 2022). Electric field simulations of single electrode *in vitro* IMT models suggest that while the coverage is sufficient for preclinical models, improvements in the extent of such coverage would be required to advance to human scale tumors (Di Sebastiano *et al* 2018, Deweyert *et al* 2019, Iredale *et al* 2020, 2022). This has been suggested through the use of multiple electrodes programmed with different relative phase shifts of the input voltage waveforms, which has been shown to theoretically increase tumor coverage and homogeneity (Iredale *et al* 2020, 2022).

Previous IMT computer simulation, optimization and treatment planning studies (Iredale *et al* 2020, 2022) have highlighted the theoretical benefit of using spatiotemporally dynamic (rotating) electric fields to increase electric field coverage over time. The optimization of relative phase shifts of input waveforms results in electric fields that rotate during the waveform period. These fields are scalable to cover human-size tumors, using low voltage waveforms (2–4 V) that produce sufficient field magnitude ($\sim$1 V cm^{-1}) to suppress human GBM cell viability (Hottinger *et al* 2016, Swanson *et al* 2016, Stupp *et al* 2017, Ballo *et al* 2019). We have shown that a previously established IMT optimization algorithm (Iredale *et al* 2020) and treatment planning system (Iredale *et al* 2022) are applicable to *in vitro*, *in vivo*, and human tumor scenarios with phase shift, voltage and electrode location optimization parameters. Rotating fields provide increased field coverage and homogeneity compared to non-rotating fields, partly explaining why rotating fields are more effective. In addition, the telophase dielectrophoresis mechanism of action suggests field direction could play a role, supported previously with analysis of cell survival versus division axis with parallel orientation showing a significant decrease in cell viability (Kirson *et al* 2004). In 2D, rotating electric fields would provide a full 360 degrees of field direction, impacting dividing cells equally, regardless of division axis. While rotating electric fields are theoretically beneficial, there has yet to be *in vitro* field measurements or investigation of the impacts on GBM cell survival. The validation of delivered electric field is imperative for accurate stimulation and requires measurement of the delivered voltage and programming adjustment for each experiment trial. In this study, the electrical conductivity of the *in vitro* media Dulbecco's Modified Eagle Medium (DMEM) was measured and employed in our computer simulations used to map the electric field. It was also used to determine the required voltage programming. An *in vitro* IMT device was designed, developed, and used to deliver rotating electric fields to patient derived GBM cells. The effects of spatiotemporally dynamic electric fields of different (a) magnitudes, (b) rotation, (c) frequency, and (d) interference were evaluated with experiments designed using supporting computer simulations. Improved field delivery validation and simulation based reprogramming methods established in this study provide a framework for future preclinical and clinical investigations. The cell response to various field patterns gives insight to the optimization goals implemented in the planning system in the future.

Methods

In vitro electrical conductivity measurement

To ensure that the desired electric field is being delivered to the target, the reduction in voltage induced by the low impedance of the culturing medium must first be considered so that the input voltage can be adjusted to account for this loss. This voltage drop is measured *in vitro* to determine the electrical conductivity and ensure that the electric field simulations are accurate. The electric fields produced from IMT electrodes *in vitro* were simulated in COMSOL Multiphysics (v5.4) at 200 kHz, where experimental geometries were replicated to provide an accurate representation of the electric field distribution over time. We measured the conductivity of our culturing media in a 3.5 cm diameter *in vitro* dish with 2 ml of DMEM at 37 °C (figure 1). A 0.25 mm diameter platinum wire electrode was placed 2.6 cm away from a grounded electrode.

We measured the impedance of the *in vitro* circuit by accounting for the internal resistance that is present in waveform generators. The relationship between the programmed input voltage V_{prog} and the voltage delivered across the load V_{meas} is dependent on the internal resistance of the waveform generator (50 Ω) and the impedance of the load Z

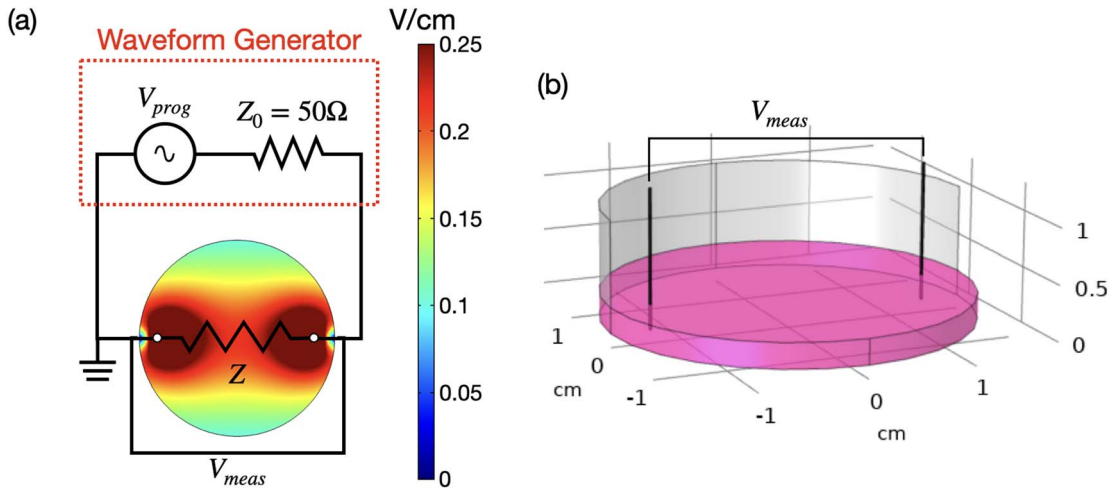

Figure 1. *In vitro* electrical conductivity measurement (a) circuit diagram with waveform generator programmed to V_{prog} and internal impedance Z_0, connected to the *in vitro* setup with impedance Z, voltage across the dish of V_{meas}, and electric field map simulated from the (b) geometry of the *in vitro* setup.

$$V_{meas} = V_{prog}\frac{Z}{Z + 50\Omega}. \quad (1)$$

The low load impedance would result in an appreciably lower measured voltage compared to the programmed voltage, requiring an adjustment to the input voltage to make up for this voltage drop. We determined the impedance of the system using the programmed voltage V_{prog} and measurements of the delivered voltage V_{meas}.

A waveform generator (Highland Technology T340 four-channel compact function generator) programmed to a 2 V amplitude sine wave at 200 kHz frequency was applied to one electrode while the other was grounded. An oscilloscope (Siglent SDS1104X-E) was used to measure the voltage amplitude when the circuit is open (V_{prog}) and when the circuit is closed (V_{meas}) (figure 1(a)), with each measurement repeated three times. The medium's electrical properties were determined by comparing the measured system impedance *in vitro* to the simulated impedance values for a range of DMEM electrical conductivities (0.1–2 S m^{-1}), and a range of permittivity constants (1–1000) computed in COMSOL.

Electrode construct design optimization

In vitro experiments to validate simulated electric field began with the choice of well size and the design of a custom four electrode IMT electrode construct. The electrode geometry containing four, 0.45 mm diameter platinum-iridium wire electrodes was created in COMSOL, along with 1 ml of DMEM with electrical conductivity determined from the *in vitro* measurement, and a dielectric constant of 80 (Arnold and Fuhr 1994, Chen *et al* 2009). In COMSOL, electrical insulation was applied on all outer boundaries and stimulating voltage controlled sinusoidal waveform ($V = A\ \sin(2\pi ft - \phi)$) terminal boundaries on the wire electrode surfaces were applied with experiment and electrode specific voltage amplitude A, phase shift ϕ, and frequency f. A tetrahedral mesh was created for the geometry for computing the electric field. Electrode separation and programming (voltage and phase shift) was determined using the custom IMT optimization algorithm (Iredale *et al* 2020, 2022) to cover the central 6 mm diameter with a homogeneous 1 V cm^{-1} time averaged electric field. The electrode separations were then used to produce the electrode construct in a 24-well plate, a well sizing that most closely represents the maximum coverable tumor diameter of 2.1 cm using four electrodes at 2 V found previously (Iredale *et al* 2020).

Experiment design optimization

The *in vitro* experiments were designed using electric field simulations. The IMT optimization algorithm (Iredale *et al* 2020, 2022) was utilized to optimize electrode voltage and phase shift programming with respect to electric field target coverage and homogeneity, and to compare different field amplitudes and programming scenarios. The voltage drop was considered in all cases, where the simulated impedance and desired voltage was used in equation (1) to determine the programmed input voltage necessary to produce the desired electric field.

The first experiment (a) investigated the electric field dose-response curve of rotating fields at 200 kHz. All models used the fixed phase shift configuration (0, $\pi/2$, π, and $3\pi/2$ radians) previously found optimal (Iredale *et al* 2020), with delivered voltage amplitudes selected for 1 V cm^{-1}, 1.5 V cm^{-1} and 2 V cm^{-1} dish coverage.

Cell survival results S were then fitted to an adapted linear quadratic (LQ) model $S = A(e^{-(\alpha E+\beta E^2)} - 1) + 1$, where E is the electric field intensity, and fit parameters of A, α and β.

The next set of experiments compared (b) rotating versus non-rotating fields at 1 V cm^{-1}, (c) 200 kHz versus 10 kHz rotating fields at 1 V cm^{-1}, and (d) constructive versus destructive interference. The rotating experimental arms used the phase shifted configuration (0, $\pi/2$, π and $3\pi/2$ radians) (Iredale *et al* 2020), with voltage amplitudes selected to cover the dish with a field of 1 V cm^{-1} at either 200 kHz (ideal frequency for GBM (Rominiyi *et al* 2021)) or 10 kHz (maximum available frequency for existing implantable stimulation devices (Megía García *et al* 2020)). The non-rotating arm contained a pair of ground and a pair of in phase stimulating electrodes with voltage selected to deliver 1 V cm^{-1} at 200 kHz, where the pattern of adjacent ground and stimulating electrodes was previously found to produce constructive interference when no phase shifting was used (Iredale *et al* 2020). A final configuration investigated the importance of field optimization and homogeneity, by using a destructive interference configuration (producing a field of 0 V cm^{-1} at the center of the region of interest) with alternating ground and stimulating electrodes at (i) the same input voltage and (ii) the same total system power as the rotating constructive interference scenario.

In vitro IMT model

GBM cells employed in this study were derived from patient tumors (Xu *et al* 2016, Di Sebastiano *et al* 2018), and had been transfected with the firefly luciferase gene to enable bioluminescence imaging (BLI) for cell viability evaluation. Two cell lines (labelled GBM23 and GBM25) were used in this study. Cells were cultured in DMEM with 10% fetal bovine serum at 37 °C, 5% CO_2, passaged at 80% confluence by splitting 1:2 using 0.25% trypsin with 0.91 mM ethylenediaminetetraacetic acid (EDTA). Culture media was changed twice weekly. GBM cells (3×10^4) were plated with 1 ml of DMEM in four wells of a 24-well plate and fitted with the custom-designed four electrode IMT delivery device. The stimulation was delivered using a four-channel waveform generator (Highland Technology T340) and a four-channel oscilloscope (Siglent SDS1104X-E) was used to validate the voltages and phase shifts delivered by each electrode. Experimental wells received continuous three-day stimulation (72 h) with experiment specific voltage and phase shift IMT waveforms applied to each electrode. Sham wells contained the electrode hardware but received no stimulation.

Cell viability was analyzed after the treatment period using BLI where 8 μl of 150 μg ml^{-1} D-luciferin (PerkinElmer) was added to the culture media, the emission intensity captured (IVIS Lumina XRMS, PerkinElmer) and the mean photon flux measured (Living Image, Xenogen). Measurement data are presented as mean $\pm$ standard deviation. Biological data sets were analyzed in MATLAB (v2022a) for normality (Öner and Deveci Kocakoç 2017), and compared using a 2-sample, 2-tailed t test, with results presented as mean $\pm$ standard error and significance assumed at $p < 0.05$.

Results

In vitro electrical conductivity measurement

Measurement of the delivered voltage *in vitro* resulted in a mean ($\pm$ standard deviation) difference $V_{prog} - V_{meas}$ of 0.14 ± 0.01 V, with voltage ratio V_{prog}/V_{meas} of 1.08 ± 0.01, corresponding to an impedance of $625 \pm 34\ \Omega$. In this model, for the range of frequencies 10–200 kHz, the impact of permittivity variations are negligible and the impedance and resistance are equivalent ($Z \approx R$), since the inverse resistance (0.0088 S) term dominates the capacitance (4.2416×10^{-12} F) term $2\pi fC$ (5×10^{-6} F s^{-1}) in the parallel RC impedance formula. With the electrical conductivity σ inversely proportional to resistance, and in our case, the impedance Z, conductivity can be expressed as $\sigma = CZ^{-1}$. The proportionality constant C is geometry dependent and was computed in COMSOL as 933.7 m^{-1} for this specific geometrical configuration (two electrodes placed 2.6 cm apart in a 3.5 cm diameter *in vitro* dish with 2 ml DMEM at 37 °C). Using this relation and the measured impedance of $625 \pm 34\ \Omega$, the conductivity of DMEM is determined to be 1.5 ± 0.1 S m^{-1}, which was then used in future *in vitro* simulations.

Electrode construct design optimization

The optimal electrode configuration was four equally spaced electrodes, each placed 6.3 mm from the center of a 1.56 cm diameter well (24-well plate). This configuration covers the well with a homogeneous 1 V cm^{-1} electric field when electrodes are programmed to deliver 1.06 V sine waves with equally spaced phase shifts (0, $\pi/2$, π and $3\pi/2$ radians). The 24-well plate provides a balance between human scale and reasonably delivered voltages (1–4 V). A custom electrode construct using this geometrical configuration was manufactured on a printed circuit board (PCB) with the capability to stimulate three dishes simultaneously with one sham dish (figure 2).

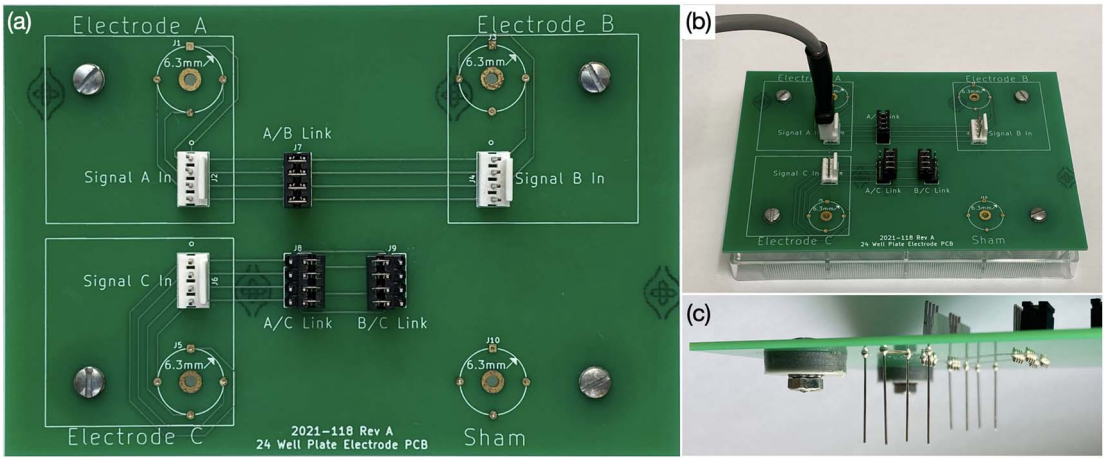

Figure 2. Custom designed printed circuit board (PCB) including (a) three stimulating electrode wells labelled 'Electrode A', 'Electrode B' and 'Electrode C', and a Sham well. Each well is individually stimulated via the Signal In connector (white) or can be connected to other wells to provide identical stimulation using the corresponding links (A/B Link, A/C Link, B/C Link). Four platinum iridium wire electrodes are included in each well, located 6.3 mm from the center. (b) PCB fitted to the 24-well plate and connected to a 4-channel waveform generator with unique stimulation delivered to each electrode in well 'Electrode A'. The A/B Link is connected in this case to provide identical stimulation to the top two wells. (c) The wire electrodes extend below the PCB, with a length that touches the bottom of the well.

Experiment design optimization

The optimal stimulation for the 200 kHz (and 10 kHz) rotating 1 V cm^{-1} average electric field in experiment (a) and (c) (figure 3) is to apply equally spaced phase shifts (0, $\pi/2$, π and $3\pi/2$ radians) to each electrode with 1.06 V amplitude sinusoidal waveforms. The impedance for this model was computed in COMSOL to be 113 Ω, with a current amplitude of 9.41 mA, and an average power of 4.99 mW per electrode, for a total of 20.0 mW for this configuration. An explanation of impedance and current calculations are included in the supplementary materials. Field magnitudes of 1.5 and 2 V cm^{-1} for this rotating field required programmed voltage increases to 1.59 and 2.12 V respectively (with an accompanying increase in current and power).

The non-rotating electric field in experiment (b) (figure 3) contains two consecutive stimulating electrodes with 0 phase shift, and two consecutive ground electrodes, and a voltage of 2.3 V applied to the two stimulating electrodes, resulting in 1 V cm^{-1} field coverage. The simulated impedance was calculated to be 225 Ω, with a current amplitude of 10.2 mA and average power of 11.7 mW per active electrode, for a total power dissipation of 23.5 mW for this configuration.

For the final experiment (d), alternating ground and 1.06 V stimulating electrodes (same voltage as rotating scenario) produced a field of 0 V cm^{-1} in the center of the dish (figure 3). This configuration resulted in an impedance of 171 Ω, current of 6.19 mA, and average power of 3.28 mW per electrode (6.56 mW total). The resulting electric field had an average 0.6 V cm^{-1} magnitude over the whole well, with the central 3 mm radius being covered with only 0.2 V cm^{-1}. Adjusting the voltage in this configuration to 1.86 V resulted in a total system power of 20.0 mW, the same as the rotating scenario, and an average electric field of 1 V cm^{-1} to the whole dish and 0.4 V cm^{-1} to the central 3 mm.

The programmed voltage required to deliver the correct voltage to the electrodes (compensating for the load impedance-induced voltage drop) was validated at the time of each experiment by measuring the delivered voltage with a four-channel oscilloscope, with results summarized in the supplementary materials (figure S1).

In vitro IMT model

Exposure of GBM23 cells to field magnitudes of 1 V cm^{-1}, 1.5 V cm^{-1} and 2 V cm^{-1} yielded field intensity dependent BLI peak signal, corresponding to mean cell viability fraction, of 0.58 ± 0.05 ($n = 6$), 0.37 ± 0.03 ($n = 6$), and 0.021 ± 0.006 ($n = 6$) relative to sham (figure 4). Cell survival results S were fit to a modified LQ model $S = A(e^{-(\alpha E + \beta E^2)} - 1) + 1$, where E is the electric field intensity, with best fit parameters to be $A = 25.1$, $\alpha = 0.012$ and $\beta = 0.0038$. This curve fit had an R-square value of 0.95.

Comparison between 200 kHz rotating and non-rotating fields at 1 V cm^{-1}, as well as 10 kHz rotating fields were analyzed for cell lines GBM23 and GBM25, where no statistical differences in cell viability were observed (figure 5). Rotating electric fields at 1 V cm^{-1} resulted in mean 0.53 ± 0.03 viability fraction ($n = 12$), non-rotating 1 V cm^{-1} fields resulted in 0.55 ± 0.06 viability ($n = 12$, $p = 0.84$), and 10 kHz rotating resulted in 0.49 ± 0.04 cell viability fraction ($n = 12$, $p = 0.39$). Applying a non-rotating electric field at the same voltage as the

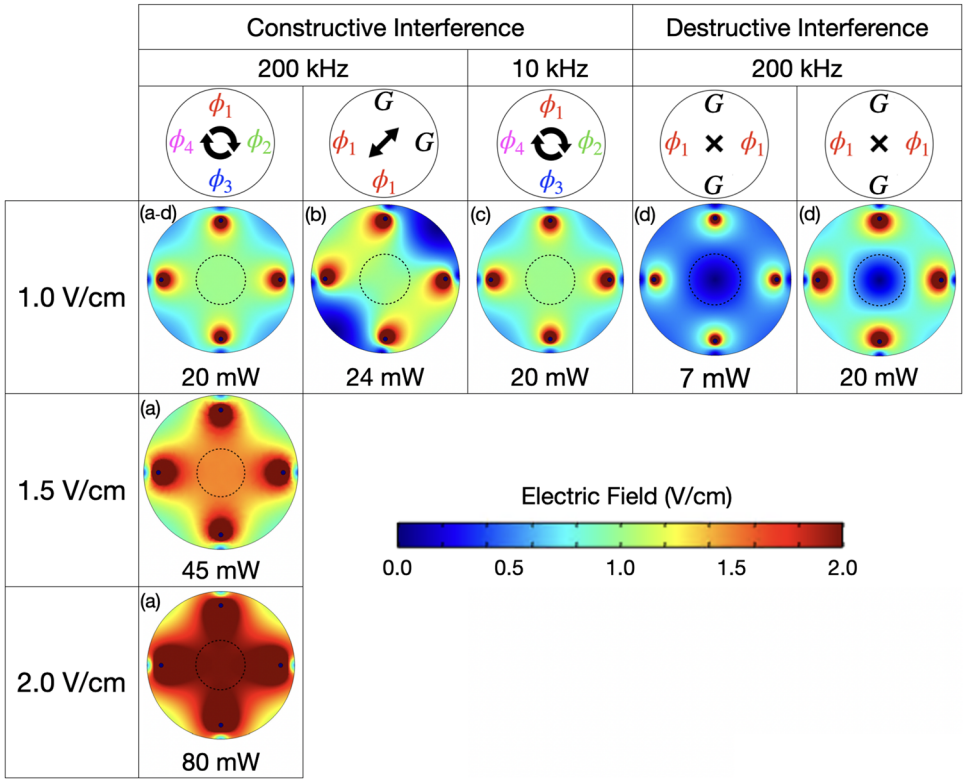

Figure 3. Summary of *in vitro* experiment designs, beginning with (a) 200 kHz rotating electric fields at magnitudes of 1, 1.5 and 2 V cm^{-1}, to determine the cell survival curve. Voltage and phase parameters were optimized for electric field coverage at the corresponding magnitude and homogeneity to the central 3 mm radius. Rotating fields were delivered with different voltage waveforms $V(t) = Asin(2\pi ft - \phi_n)$ to each electrode ($n = 1, 2, 3, 4$), where A is the voltage amplitude, t is time, f is the frequency, and ϕ_n is the phase shift. Experiment (b) compares field rotation to no rotation by grounding (G) two adjacent electrodes and (c) compares a different rotating field frequency of 10 kHz, all with voltage configurations optimized to cover the central 3 mm radius with 1 V cm^{-1}. (d) Destructive interference configurations contain alternating ground (G) and stimulating electrodes: voltage matched (left) or power matched (right) to the rotating scenario, resulting in a field cancellation to 0 V cm^{-1} in the center. See figure S3 for animation of this figure.

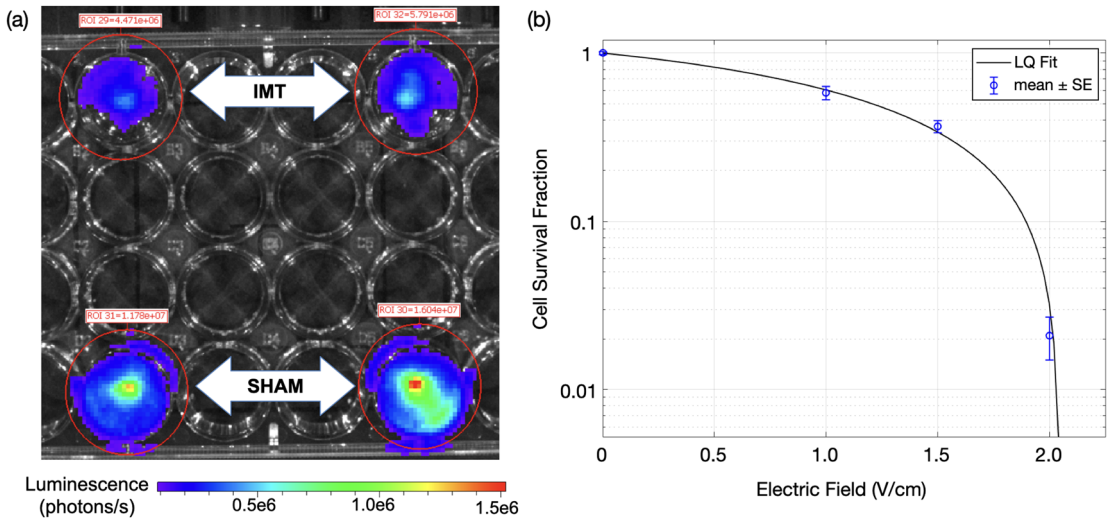

Figure 4. (a) Bioluminescence image after 3 d of 1.5 V cm^{-1} average IMT electric fields to the top two wells. Bottom two wells were not stimulated, to provide two sham conditions. (b) The cell survival curve for increasing electric field magnitudes. Data is plotted as the mean ± standard error in blue, and the data was fit to a linear quadratic model $S = A(e^{-(\alpha E + \beta E^2)} - 1) + 1$ in black ($R^2 = 0.95$).

rotating case, but with destructive interference at 200 kHz to both cells lines resulted in a mean 0.99 ± 0.02 ($n = 12$) cell viability fraction relative to sham, statistically significant compared to the optimized rotating case with 0.53 ± 0.03 viability relative to sham ($p < 0.001$). Using the same power consumption as the rotating case,

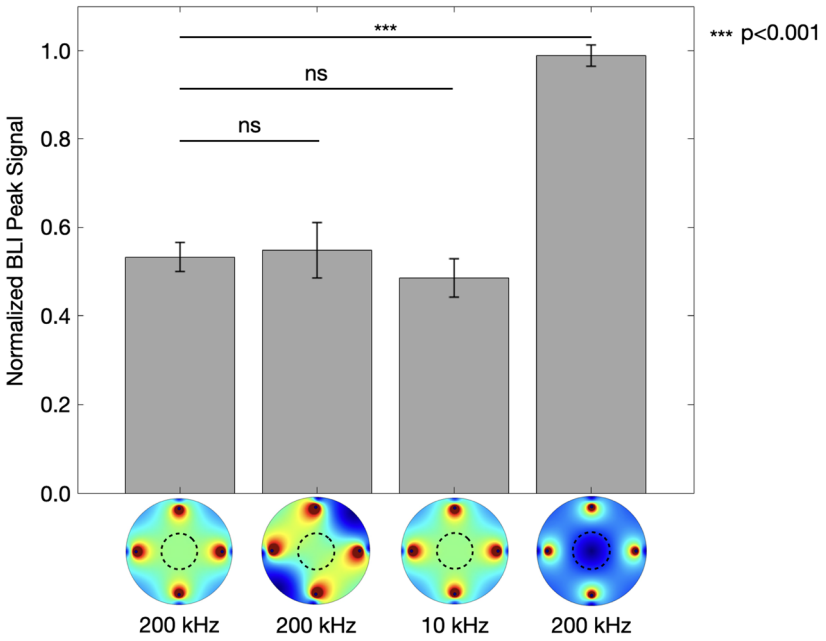

Figure 5. Mean of the BLI peak signal normalized to sham ± standard error, proportional to the cell survival, for the cases of constructive interference 200 kHz rotating fields (0.53 ± 0.03, $n = 12$), 200 kHz non-rotating (0.55 ± 0.06, $n = 12$), 10 kHz rotating fields (0.49 ± 0.04, $n = 12$), and destructive interference 200 kHz voltage matched non-rotating fields (0.99 ± 0.02, $n = 12$).

the destructive interference model applied to GBM23 cells resulted in a mean 0.66 ± 0.03 viability relative to sham, statistically significant ($n = 6$, $p < 0.01$) when compared to the rotating case performed in parallel, with 0.47 ± 0.04 viability relative to sham (figure 6).

Discussion

In this study, the theoretical improvement to target coverage and homogeneity from rotating electric fields generated by multiple electrodes was investigated *in vitro* for the first time. The impact of spatiotemporally dynamic electric fields on GBM cell viability was investigated by first validating that the desired electric field was delivered to preclinical models, by adjusting the programmed voltage to account for the voltage drop. The measured delivered voltage for a two-electrode *in vitro* scenario was used to determine the electrical conductivity of the *in vitro* media as 1.5 ± 0.1 S m^{-1}, using a geometrically accurate COMSOL simulation model. With the electrical conductivity known, COMSOL simulations can be used to determine the necessary applied voltage that is required to produce the desired electric field at the target. For preclinical experiments, the simulated voltage adjustment was also validated prior to stimulation by measuring the delivered voltage to the circuit. The electrical conductivity for DMEM computed in this study was compared to values presented in the literature. Due to the temperature sensitivity of electrical conductivity, only literature comparisons at 37 °C were considered. Furthermore, below 10 MHz, electrolytic conductivity is considered frequency independent (Grimnes and Martinsen 2014). Compared to the value for DMEM of 1.5 ± 0.1 S m^{-1} determined in Results section *A*; the literature value of 1.4 ± 0.1 S m^{-1} (Chen *et al* 2009) matches our measurement within the uncertainty.

Computer simulations of the *in vitro* experimental model, used in conjunction with the IMT optimization algorithm to design a four-electrode IMT device provided a platform to demonstrate the impact of rotational fields. Electrodes placed 6.3 mm from the center of a 24-well plate most closely represented the largest spherical tumor volume coverable with four electrodes, previously found to be a 2.1 cm diameter tumor with electrodes places 7.5 mm from the center (Iredale *et al* 2020). For this geometry to produce optimal fields, each electrode must be separately programmable, a key feature of the IMT PCB and accompanying four-channel waveform generator. Expansion to the use of multiple electrodes in IMT has been theoretically supported (Iredale *et al* 2020, 2022), with the impact on cell viability investigated for the first time in this work.

The custom IMT *in vitro* delivery device and experiments were implemented on patient derived GBM cell lines and cell viability was observed with BLI. Rotating fields were effective at reducing cell viability in a field intensity dependent manner. Cell survival results S were fit to a modified LQ model with an R-square value of 0.95. This data fit suggests that, similar to radiotherapy, cells exposed to IMT fields have intrinsic linear and

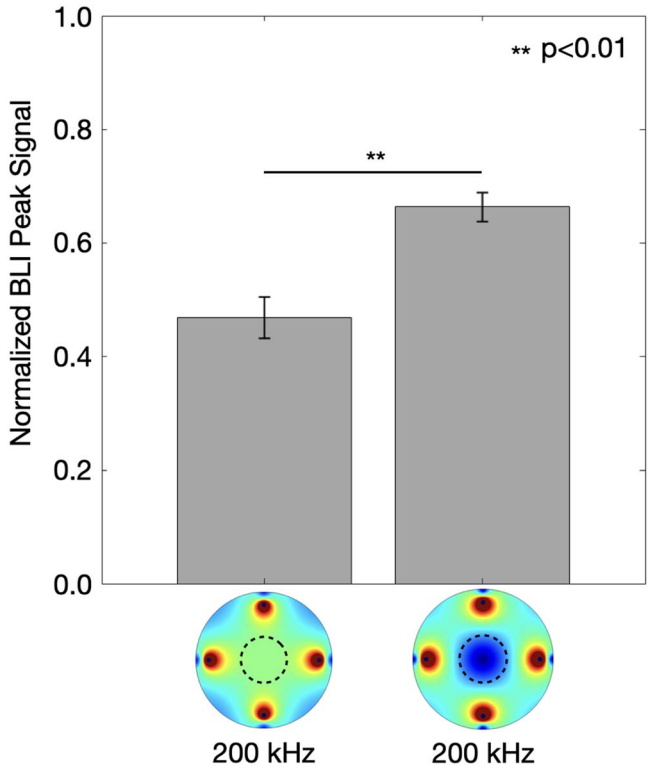

Figure 6. Mean of the BLI peak signal normalized to sham ± standard error, proportional to the cell survival, for the cases of constructive interference 200 kHz rotating fields (0.47 ± 0.04, $n = 6$) and destructive interference power matched (0.66 ± 0.03, $n = 6$).

quadratic parameters, α and β, that influence cell survival (figure 4). With efficacy found to be dependent on not only field intensity, but field direction and exposure time (Korshoej *et al* 2019), it is important to consider such factors. Current external electric field devices provide only two field directions and have just begun to consider the impact of fractional anisotropy in the brain on the resulting intratumoral electric field. For *in vitro* studies such as the current investigation, fractional anisotropy is not present, but when expanding IMT to patient models, the fractional anisotropy should be considered for impacts on rotating fields applied with intratumoral electrodes.

We did not find statistical difference in response between the spatiotemporal dynamic rotating electric field case versus the non-rotating case with both delivering the same field magnitude within the 3 mm radius in the center. However, the optimized rotating field had almost 20% lower power consumption (20.0 mW) compared to the non-rotating case (23.5 mW). We also noted that the non-rotating case exhibited field cancellations on the edges of the well, whose impact would be considerable for targets exceeding ~3 mm radius. For the above reasons, spatiotemporally dynamic fields are preferred over their non-rotating counterparts. Interestingly, cell viability was not significantly different between 200 kHz and 10 kHz rotating fields, suggesting that previously thought inefficacious frequencies (Kirson *et al* 2004, 2007, Wenger *et al* 2015, Berkelmann *et al* 2019) could be effective with the rotating paradigm in certain cell lines. Furthermore, when we compared the two cell lines, the survival of GBM23 and GBM25 cells were not significantly different for the 200 kHz rotating scenario (58 ± 5% versus 48 ± 3%) ($p = 0.13$), the 10 kHz scenario (54 ± 7% versus 43 ± 5%) ($p = 0.23$), or the destructive interference voltage matched case (97 ± 4% versus 101 ± 3%) ($p = 0.45$) but were significantly different (69 ± 6% versus 40 ± 7%) for the non-rotating scenario ($p = 0.01$) (figure S2).

Through destructive interference, we created a central 'cold zone' of 0.2 V cm^{-1} in the central 3 mm radius of a well with average 0.6 V cm^{-1} field, by using the same stimulation voltages as the rotating electric field case, yielding 99 ± 2% viability experimentally. We then applied the same system power and whole well electric field (1 V cm^{-1}) as the rotating case, with a central field of 0.4 V cm^{-1}, yielding 66 ± 3% cell viability experimentally, compared to 47 ± 4% for the rotating case. This suggests that even though we applied the same stimulation voltages, or the same system power, optimization of field homogeneity is critical for IMT field planning, and supports the methods previously established in IMT optimizations (Iredale *et al* 2020, 2022).

Evaluating the efficacy of spatiotemporally dynamic fields experimentally provides insight for future treatment planning optimization goals. Both field coverage and homogeneity will continue to be included as the objective goals with optimization parameters of phase shift, voltage, and electrode placement. Incorporation of

field rotation minimizes both field cold spots and power consumption. These qualities are impactful when translating IMT to the patient setting, where maximum coverage with minimal input current is vital to maximizing battery life of IMT implantable waveform generators. We can always do more: more replicates, more cell lines, and/or more comparisons, but we hope we have satisfactorily demonstrated how we designed and implemented a PCB that made performing *in vitro* experiments with multi-electrode stimulations consistent.

Conclusion

In this proof-of-concept study, the improved impact of electric field optimization was supported through *in vitro* GBM cell survival analysis. Electrical conductivity measurement of DMEM provided accurate optimizable computer simulations, used to determine required voltage, and calculate current and power. *In vitro* experiments designed and applied to patient derived GBM cells highlighted the considerations and effectiveness of using computerized optimization techniques to design subject-specific spatiotemporally dynamic IMT electric fields that minimize power delivered and cold spots within the treatment fields. With a patient-specific dose response of rotating electric fields established, future IMT studies can compare variation between patients, and determine the necessary inputs required for optimization techniques. The concept of spatiotemporally dynamic fields created through optimizing stimulation parameters can be utilized in future translational applications in rodents and patients, to further IMT development.

Acknowledgments

This work is supported in part by NSERC CGS-D (EI), NSERC Idea to Innovation Grant (EW), NSERC Discovery Grant (EW), Cancer Research Society (MOH), the Canada Foundation for Innovation (CFI) (TP) and the Western Innovation Fund (MOH).

Data availability statement

The data cannot be made publicly available upon publication because they are not available in a format that is sufficiently accessible or reusable by other researchers. The data that support the findings of this study are available upon reasonable request from the authors.

Ethical statement

Human ethics approval: REB #17290

Western University REB operates in compliance with, and is constituted in accordance with, the requirements of the TriCouncil Policy Statement: Ethical Conduct for Research Involving Humans (TCPS 2); the International Conference on Harmonisation Good Clinical Practice Consolidated Guideline (ICH GCP); Part C, Division 5 of the Food and Drug Regulations; Part 4 of the Natural Health Products Regulations; Part 3 of the Medical Devices Regulations and the provisions of the Ontario Personal Health Information Protection Act (PHIPA 2004) and its applicable regulations. The REB is registered with the U.S. Department of Health & Human Services under the IRB registration number IRB 00000940.

Biosafety: BSP-LHSC-007

Conflicts of Interest

MOH and SS are inventors on the following patent that is assigned to 'London Health Sciences Centre Research Inc.' (the applicant): CA2985847 entitled 'Intratumoral Modulation Therapy'. EW, MOH, TP and SS are inventors on the following patent application that is assigned to 'London Health Sciences Centre Research Inc.' (the applicant): WO2021142549 entitled 'Planning and delivery of dynamically oriented electric field for biomedical applications'. The authors have no other competing interests.

ORCID iDs

Eugene Wong https://orcid.org/0000-0001-6869-0122

References

Arnold W M and Fuhr G 1994 Increasing the permittivity and conductivity of cellular electromanipulation media *IEEE Industry Applications Society Annual Meeting* 2, 1470–6

Ballo M T, Urman N, Lavy-Shahaf G, Grewal J, Bomzon Z and Toms S 2019 Correlation of tumor treating fields dosimetry to survival outcomes in newly diagnosed glioblastoma: a large-scale numerical simulation-based analysis of data from the Phase 3 EF-14 randomized trial *Int. J. Radiat. Oncol.* **104** 1106–13

Berkelmann L, Bader A, Meshksar S, Dierks A, Majernik G H, Krauss J K, Schwabe K, Manteuffel D and Ngezahayo A 2019 Tumour-treating fields (TTFields): investigations on the mechanism of action by electromagnetic exposure of cells in telophase/cytokinesis *Sci. Rep.* **9** 1–117362

Chen M-T, Jiang C, Vernier P T, Wu Y-H and Gundersen M A 2009 Two-dimensional nanosecond electric field mapping based on cell electropermeabilization *PMC Biophys.* **2** 1–169

Deweyert A, Iredale E, Xu H, Wong E, Schmid S and Hebb M O 2019 Diffuse intrinsic pontine glioma cells are vulnerable to low intensity electric fields delivered by intratumoral modulation therapy *J. Neuro-Oncol.* **143** 49–56

Di Sebastiano A R, Deweyert A, Benoit S, Iredale E, Xu H, de Oliveira C, Wong E, Schmid S and Hebb M O 2018 Preclinical outcomes of intratumoral modulation therapy for glioblastoma *Sci. Rep.* **8** 1–11

Fabian D, Guillermo Prieto Eibl MdP, Alnahhas I, Sebastian N, Giglio P, Puduvalli V, Gonzalez J and Palmer JD 2019 Treatment of glioblastoma (GBM) with the addition of tumor-treating fields (TTF): a review *Cancers* **11** 1–12

Grimnes S and Martinsen Ø G 2014 *Bioimpedance and Bioelectricity Basics* (Amsterdam: Elsevier) 3rd edn 9780124115330

Hottinger A F, Pacheco P and Stupp R 2016 Tumor treating fields: a novel treatment modality and its use in brain tumors *Neuro Oncol.* **18** 1338–49

Iredale E, Deweyert A, Hoover D A, Chen J Z, Schmid S, Hebb M O, Peters T M and Wong E 2020 Optimization of multi-electrode implant configurations and programming for the delivery of non-ablative electric fields in intratumoral modulation therapy *Med. Phys.* **47** 5441–54

Iredale E, Voigt B, Rankin A, Kim K W, Chen J Z, Schmid S, Hebb M O, Peters T M and Wong E 2022 Planning system for the optimization of electric field delivery using implanted electrodes for brain tumor control *Med. Phys.* **49** 6055–67

Kirson E D, Gurvich Z, Schneiderman R, Dekel E, Itzhaki A, Wasserman Y, Schatzberger R and Palti Y 2004 Disruption of cancer cell replication by alternating electric fields *Cancer Res.* **64** 3288–95

Kirson E D, Dbalý V, Tovaryš F, Vymazal J, Soustiel J F, Itzhaki A, Mordechovich D, Steinberg-Shapira S, Gurvich Z, Schneiderman R, Wasserman Y, Salzberg M, Ryffel B, Goldsher D, Dekel E and Palti Y 2007 Alternating electric fields arrest cell proliferation in animal tumor models and human brain tumors *Proc. Natl Acad. Sci.* **104** 10152–7

Korshoej A R, Hansen F L, Thielscher A, von Oettingen G B and Sørensen J C H 2017 Impact of tumor position, conductivity distribution and tissue homogeneity on the distribution of tumor treating fields in a human brain: a computer modeling study *PLoS One* **12** 1–21 e0179214

Korshoej A R, Saturnino G B, Rasmussen L K, von Oettingen G, Sørensen J C H and Thielscher A 2016 Enhancing predicted efficacy of tumor treating fields therapy of glioblastoma using targeted surgical craniectomy: a computer modeling study *PLoS One* **11** 1–25 e0164051

Korshoej A R, Sørensen J C H, von Oettingen G, Poulsen F R and Thielscher A 2019 Optimization of tumor treating fields using singular value decomposition and minimization of field anisotropy *Phys. Med. Biol.* **64** 1–9

Lok E, San P, Hua V, Phung M and Wong E T 2017 Analysis of physical characteristics of tumor treating fields for human glioblastoma *Cancer Med.* **6** 1286–300

Megía García A, Serrano-Muñoz D, Taylor J, Avendaño-Coy J and Gómez-Soriano J 2020 Transcutaneous spinal cord stimulation and motor rehabilitation in spinal cord injury: a systematic review *Neurorehabil Neural Repair.* **34** 3–12

Miranda P C, Mekonnen A, Salvador R and Basser P J 2014 Predicting the electric field distribution in the brain for the treatment of glioblastoma *Phys. Med. Biol.* **59** 4137–47

Nam J Y and de Groot J F 2017 Treatment of Glioblastoma *J. Oncol. Pract.* **13** 629–38

Öner M and Deveci Kocakoç İ 2017 JMASM 49: a compilation of some popular goodness of fit tests for normal distribution: their algorithms and MATLAB codes (MATLAB) *J. Mod. Appl. Stat. Methods.* **16** 547–75

Rominiyi O, Vanderlinden A, Clenton S J, Bridgewater C, Al-Tamimi Y and Collis S J 2021 Tumour treating fields therapy for glioblastoma: current advances and future directions *Br. J. Cancer* **124** 697–709

Shah P P, White T, Khalafallah A M, Romo C G, Price C and Mukherjee D 2020 A systematic review of tumor treating fields therapy for high-grade gliomas *J. Neuro-Oncol.* **148** 433–43

Stupp R, Taillibert S, Kanner A *et al* 2017 Effect of tumor-treating fields plus maintenance temozolomide vs maintenance temozolomide alone on survival in patients with glioblastoma *JAMA* **318** 2306–16

Swanson K D, Lok E and Wong E T 2016 An overview of alternating electric fields therapy (novottf therapy) for the treatment of malignant glioma *Curr. Neurol.Neurosci. Rep.* **16** 1–10

Wenger C, Miranda P C, Salvador R, Thielscher A, Bomzon Z, Giladi M, Mrugala M M and Korshoej A R 2018 A review on tumor-treating fields (TTFields): clinical implications inferred from computational modeling *IEEE Rev. Biomed. Eng.* **11** 195–207

Wenger C, Giladi M, Bomzon Z, Salvador R, Basser P J and Miranda P C 2015 Modeling tumor treating fields (TTFields) application in single cells during metaphase and telophase *2015 37th Annual Int. Conf. of the IEEE Engineering in Medicine and Biology Society (EMBC)* pp 6892–5

Wenger C, Salvador R, Basser P J and Miranda P C 2015 The electric field distribution in the brain during TTFields therapy and its dependence on tissue dielectric properties and anatomy: a computational study *Phys. Med. Biol.* **60** 7339–57

Xu H, Bihari F, Whitehead S, Wong E, Schmid S and Hebb M O 2016 *In vitro* validation of intratumoral modulation therapy for glioblastoma *Anticancer Res.* **36** 71–80